Myosin phosphatase target subunit 1 **governs integrity of the embryonic gut epithelium to circumvent atresia development in medaka,** ***Oryzias latipes***

Daisuke Kobayashi[1,*], Kazuhiko Matsuo[1], Tetsuaki Kimura[2], Satoshi Ansai[3], Hayato Yokoi[4], Shigeo Takashima[5], Tadao Kitagawa[6], Takahiro Kage[7], Takanori Narita[8], Tomoko Jindo[7] Masato Kinoshita[9], Kiyoshi Naruse[10], Yoshiro Nakajima[1], Masaki Shigeta[1], Shinichiro Sakaki[1], Satoshi Inoue[1], Rie Saba[11], Kei Yamada[11], Takahiko Yokoyama[1], Yuji Ishikawa[12], Kazuo Araki[13], Yumiko Saga[7,14,15,], Hiroyuki Takeda[7,*], Kenta Yashiro[1,*]

[1]Department of Anatomy and Developmental Biology, Kyoto Prefectural University of Medicine, 465 Kajii-cho, Kamigyo-ku, Kyoto 602-8566, Japan.

[2]Human Genetics Laboratory, National Institute of Genetics, 1111 Yata, Mishima, Shizuoka, Japan

[3]Graduate School of Life Sciences, Tohoku University, Sendai 980-8577, Japan

[4]Graduate School of Agricultural Science, Tohoku University, Sendai 980-8572, Japan.

[5]Institute for Glyco-core Research (iGCORE)/Life Science Research Center, Gifu University, 1-1 Yanagido, Gifu 501-1193, Japan

[6]Program in Environmental Management, Graduate School of Agriculture, Kindai University, 3327-204 Nakamachi, Nara, Nara 631-8505, Japan.

[7]Department of Biological Sciences, Graduate School of Science, The University of Tokyo, Bunkyo-ku, Hongo, Tokyo, 113-0033 Tokyo, Japan

[8]Laboratory of Molecular Biology, Department of Veterinary Medicine, College of Bioresource Sciences, Nihon University, 1866 Kameino, Fujisawa, Kanagawa 252-0880, Japan.

[9]Department of Applied Biosciences, Graduate School of Agriculture, Kyoto University, Kyoto 606-8502, Japan

[10]Laboatory of Bioresources, National Institute for Basic Biology, 38 Nishigonaka, Myodaiji, Okazaki 444-8585 Aichi, Japan

[11]Department of Radiology, Kyoto Prefectural University of Medicine, 465 Kajii-cho, Kamigyo-ku, Kyoto 602-8566, Japan.

[12]Research Center for Radiation Protection, National Institute of Radiological Sciences, 4-9-1 Anagawa, Inage-ku, Chiba 263-8555, Japan.

[13]Research Center for Aquatic Breeding, National Research Institute of Aquaculture, Fisheries Research Agency, 224 Hiruda, Tamaki-cho, Watarai, Mie 519-0423, Japan.

[14]Department of Gene Function and Phenomics, Mammalian Development Laboratory, National Institute of Genetics, Mishima 411-8540, Japan.

[15]Department of Genetics, The Graduate University for Advanced Studies, SOKENDAI, Mishima 411-8540, Japan

*Address correspondence to: Daisuke Kobayashi (kdaisuke@koto.kpu-m.ac.jp), Hiroyuki Takeda (htakeda@bs.s.u-tokyo.ac.jp) and Kenta Yashiro (kyashiro@koto.kpu-m.ac.jp)

Running title: Intestinal atresia in medaka (*O. latipes*)

Keywords: intestinal atresia, disease model, actomyosin regulation, intestinal development

Bullet Points:

- Medaka *mypt1* mutants display intestinal atresia.
- The level of phosphorylated myosin regulatory light chain was higher in *mypt1* mutant embryos than in *wild-type* embryos.

- The levels of F-actin appeared elevated in the intestinal epithelium of *mypt1* mutants.
- Blebbistatin, an inhibitor of non-muscle myosin II, rescued intestinal atresia in *mypt1* mutant embryos.

Conflict of interest disclosure: The authors declare no competing interests.

Funding statement: This work was supported by JSPS (Japan Society for the Promotion of Science) KAKENHI Grant # 15K08139 and 21K08601 and NIBB Individual Collaborative Research Program (14-376) to DK.

Abstract

Background: Intestinal atresia (IA) is a congenital gut obstruction caused by the absence of gut opening. Genetic factors are assumed to be critical for the development of IA, in addition to accidental vascular insufficiency or mechanical strangulation. However, the molecular mechanism underlying IA remains poorly understood.

Results: In this study, to better understand such a mechanism, we isolated a mutant of *Oryzias latipes* (the Japanese rice fish known as medaka) generated by N-ethyl-N-nitrosourea mutagenesis, in which IA develops during embryogenesis. Positional cloning identified a nonsense mutation in the *myosin phosphatase target subunit 1* (*mypt1*) gene. Consistent with known Mypt1 function, the active form of myosin regulatory light chain (MRLC), which is essential for actomyosin contraction, and F-actin were ectopically accumulated in the intestinal epithelium of mutant embryos, whereas cell motility, proliferation and cell death were not substantially affected. Corresponding to the accumulation site of F-actin/active

MRLC, the intestinal epithelium architecture was disordered. Importantly, blebbistatin, a non-muscle myosin inhibitor, attenuated the development of IA in the mutant.

Conclusions: Cytoskeletal contraction governed by *mypt1* regulates the integrity of the embryonic intestinal epithelium. This study provides new insight into our understanding of the mechanism of IA development in humans.

Introduction

Intestinal atresia (IA) is a birth defect of the intestine defined as a complete blockage of the intestinal lumen. It occurs in approximately 1.3:10,000 to 2.9:10,000 newborns, and affected individuals require surgical repair for survival.[1] In many cases, the lack of local blood supply to the developing embryonic gut because of a vascular defect has been regarded as being responsible for IA.[2,3] However, familial cases and a higher incidence among 21 trisomy patients indicate a genetic cause.[3-6] Recently, a null mutation of *Fgfr2IIIb* or its ligand *Fgf10* has been reported to cause IA without mesenteric vascular occlusion in mice, although such a genetic defect has not been reported in human cases.[7-10] Thus, the molecular mechanism underlying IA appears to be etiologically heterogeneous and remains largely unknown.

Intestinal morphogenesis in *Oryzias latipes*, the Japanese rice fish known as medaka, requires the medial migration of the endoderm epithelial monolayer overlying the yolk syncytial layer to the ventral midline at stage (st.) 21.[11] This monolayer endoderm epithelium develops into a bilayer with the shape of each cell elongating mediolaterally. Then, the anterior gut portion behaves differently from the intermediate and posterior gut portions. Cells in the anterior part stack up and converge on the dorsal midline to form the endodermal rod of the intestinal anlage, and organize into a radial configuration. However, in the intermediate and posterior positions, each cell elongates dorsoventrally and then internally

cavitates to form a gut tube. Tube formation itself develops in an orderly fashion, in an anterior to posterior direction. The anterior and intermediate intestine has a lumen at st. 25, and tube formation in the posterior portion is completed at st. 26. During this process, buds of accessory organs, such as the liver and swim bladder, morphologically appear.[11]

Contraction of the actomyosin cytoskeleton, which is dependent on non-muscle myosin II (NMII), is central to morphogenesis by affecting cell shape, adhesion and migration, and tissue architecture.[12,13] Phosphorylation of myosin regulatory light chain (MRLC) triggers actomyosin contractility.[14] Thus, the molecular mechanism regulating phosphorylated-MRLC (pMRLC) is key to morphogenesis. Myosin light chain phosphatase (MLCP) dephosphorylates pMRLC, which promotes actomyosin relaxation. MLCP is a heterotrimer composed of catalytic subunit of type 1 phosphatase δ (PP1cδ), myosin phosphatase target subunit 1 (Mypt1, also known as protein phosphatase 1 regulatory subunit 12a: Ppp1r12a) and a small subunit, M20.[15] Mypt1 alters the conformation of the catalytic domain of MLCP, conferring substrate specificity and increasing enzyme activity.[16,17] Mypt1 is critical for gastrulation, axon guidance, vascular remodeling, and morphogenesis/patterning of the liver, pancreas, and central nervous system.[18-25]

In this study, to better understand the genetic and molecular basis of IA, we identified a medaka mutant in which IA develops during embryogenesis. This mutant was isolated through N-ethyl-N-nitrosourea (ENU) mutagenesis screening.[26] Positional cloning identified a nonsense mutation in *mypt1* in this mutant. During embryogenesis, endoderm cells behaved properly in the mutant to form the gut anlage. However, the anlage became discontinued along the anteroposterior axis of the intermediate portion resulting in IA, just after the formation of a gut lumen was completed. Consistent with known Mypt1 function, cytoskeletal actomyosin contraction was indicated to be higher at the lesion. Our study

provides a novel platform to examine the integrity of the embryonic endodermal gut epithelium and the pathological molecular mechanism underlying IA.

Results

The *g1-4* medaka mutant develops IA

The *g1-4* medaka mutant was isolated as a recessive lethal line through our ENU mutagenesis screen for mutations affecting embryonic development and organogenesis.[26] Examination of mutant embryos identified IA, which developed at st. 32–33 in homozygous mutants, although the penetrance of the IA phenotype varied and did not reach 100% (Table 1). Medaka have small and large intestines that are discerned from each other morphologically as well as by specific gene expression profiles in adults.[27] However, we could not distinguish small from large intestine in the embryos according to morphology or by the expression of molecular markers. Therefore, hereafter, we simply define the region between the liver bud and the cloaca as intestine. Despite of the existence of IA, the remaining intestine appeared to be properly developed at st. 40, the hatching sage (Fig. 1A, B).

The *g1-4* allele encodes *mypt1*

We hypothesized that the inheritance mode of the *g1-4* mutant was recessive and to identify the locus affected we performed positional cloning. We first mapped it to linkage group 23 (LG23) using M-marker analysis.[28] Subsequently, we performed high-resolution linkage analysis using an F2 mapping panel (766 embryos). This confined *g1-4* to reside in a 0.13 cM interval between the markers LG23-4.4 and LG23-4.6, a region of 24.227 kb (Fig. 1C). A survey of this region of the medaka reference genome sequence identified only one gene, *mypt1*, also known as *ppp1r12a* (*protein phosphatase 1 regulatory subunit 12a*).

The open reading frame (ORF) of medaka *mypt1* (3,234 bp: DDBJ accession number, LC662536) consists of 25 exons. Mypt1 protein is predicted to be 1078 amino acids long and is closely related to human MYPT1 (NP_001137357.1). Medaka Mypt1 has three highly

conserved domains, an RVxF motif, an ankyrin repeat, and a protein kinase cGMP-dependent (PRKG) interacting domain (Fig. 1D). Sequencing the *g1-4* allele revealed a C to A transversion in exon 22 (C2952A), which introduces a premature stop codon (Fig. 2C, D). The predicted premature termination of Mypt1 in the *g1-4* mutant occurs inside the PRKG interacting domain. This results in deletion of the C-terminal leucine-zipper (LZ) motif, which is essential for interaction with PRKG1α.[16,29] Interaction between Mypt1 and PRKG1α is essential for actomyosin activation; therefore, C2952A is expected to perturb the function of Mypt1.

To confirm whether the mutation in *mypt1* is responsible for IA in the *g1-4* mutants, we tried to rescue the mutant using *wild-type* (*WT*) *mypt1* mRNA. Unfortunately, for reasons unknown, we could not synthesize the full-length *mypt1* mRNA *in vitro*. Alternatively, we generated *mypt1* knockout medaka using the CRISPR/Cas9 system.[30] We isolated a mutant line possessing an 11 nucleotide deletion with a 7 nucleotide insertion (*mypt1*$^{\#4\text{-}6}$, c.127_137delinsTCTGTAT, Fig. 1D, Fig. 2A). This mutation creates a transcriptional frame shift that alters 45 codons before introducing a premature stop codon at the 88th codon. The F1 pair spawned IA embryos at 23.7% of total siblings (n = 59) and we successfully maintained a mutant line. In the F2 generation, the penetrance varied among pairs as observed in the original mutagenesis line (Table 2). Approximately 15–30% of total siblings showed an IA phenotype, a higher penetrance than in the original mutant. For further phenotypic analysis, we used this newly generated mutant line, *mypt1*$^{\#4\text{-}6}$. We could also see dilation of the intestine upstream of the atresia, which is generally observed in IA cases, at the hatching stage in *mypt1*$^{\#4\text{-}6}$ embryos (Fig. 3A–D). Thus, given these findings, we concluded that *mypt1* mutation is responsible for the IA phenotype.

Apart from the atresia legion, the *mypt1*$^{\#4\text{-}6}$ intestine possesses intact developmental competence

To further examine the epithelial architecture of *mypt1*$^{\#4\text{-}6}$ mutant intestine, we performed histological analysis. Apart from IA, the embryonic intestine appeared intact in the *mypt1*$^{\#4\text{-}6}$ mutant. The mesenchymal cells giving rise to smooth muscle cells and connective tissue surrounded the endodermal epithelium layer as in developing *WT* intestine (Fig. 3F–M and 4Aa–Gb).[31] Cytokeratin, an intermediate filament molecule, is an epithelial cell marker that predominantly localizes to the apical plasma membrane if polarized.[32] Consistent with this, the gut epithelium of st. 31 *WT* embryos showed definite apical distribution of cytokeratin (Fig. 4Bb). In *mypt1*$^{\#4\text{-}6}$ embryos, intestinal epithelium in areas other than the IA lesion had the same subcellular distribution of cytokeratin as the *WT* (Fig. 4Cb). Smooth muscle cells, represented by smooth-muscle-specific myosin (SM-myosin), properly surrounded the intestinal epithelium in *WT* and *mypt1*$^{\#4\text{-}6}$ embryos at st. 31 (Fig. 4Ba–Cb). Interestingly, in the mutant, the blind-end of the atresia lesion was lined by a smooth muscle layer. The basement membrane, represented by laminin, underlying the epithelial basal surface developed properly in the mutant, even at the blind-end of the atresia lesion (Fig. 5Da–Eb). These results indicated that the fundamental structure of the gut, including the apical-basolateral polarity of the intestinal epithelium and muscle layer, developed normally except for the atresia, which is consistent with human IA cases.

We next elucidated how the intestine is altered through atresia formation in *mypt1*$^{\#4\text{-}6}$ embryos. Despite continuous and careful observation of live fish we could not diagnose IA morphologically until st. 28.

The expression pattern of *forkhead box protein a2* (*foxa2*), which is expressed in the endoderm and its derived organs including intestine[11], was indistinguishable between *WT* and mutant embryos until st. 26 (Fig. 5).[11] This indicates that a defect of early endoderm

formation and/or migration is not a cause of IA in *mypt1*$^{\#4\text{-}6}$ mutants. However, in the mutant embryos, intestinal epithelium expressing *foxa2* had a gap in continuity along the anteroposterior axis at st. 27, which is a likely sign of developing IA (Fig. 5L). Importantly, at st. 26, when intestinal tube formation completes,[11] fragmentation of the basement membrane was seen in the mutant intestine, indicating the initial event of IA formation (Fig. 4Fa–Gb). Taken together, the molecular event underlying the pathogenesis of IA in this mutant had already started at st. 26, although the morphological anomaly was not obvious.

Next, we examined whether a cell death or proliferation defect causes disintegration of intestinal epithelium, in the form of basement membrane fragmentation, in *mypt1* mutants. TUNEL assays revealed that apoptotic cells were rare in both *WT* and *mypt1*$^{\#4\text{-}6}$ intestine at st. 26 (Fig 6A, B). Additionally, we could not see any significant difference in proliferative ability between *WT* and mutant intestine, represented by the number of the metaphase cells (Fig. 6E–I). Thus, we concluded that cell death and/or altered cell proliferation is not responsible for basement membrane fragmentation and IA development.

Even though apical-basolateral polarity is established in the gut epithelium anlage, epithelial-mesenchymal transition (EMT) may cause local depletion of apical-basolateral polarity and fragmentation of the basement membrane, as in gastrulation.[33] We, therefore, examined this possibility. It is well known that *snail family zinc finger* (*snai*) *1a*, *snai1b* and *snai2* induce EMT.[34] Whole mount *in situ* hybridization did not show any expression of *snai1a*, *snailb* or *snai2* in *WT* or mutant intestine at stage 26 (Fig. 6J–O). Consistently, subcellular localization of Pkcζ, an apical epithelium marker, was not disturbed in *mypt1*$^{\#4\text{-}6}$ intestine at st. 26 (Fig. 4Ha–Ib). These observations are consistent with the absence of cytokeratin downregulation, which is observed in EMT (Fig. 4Ba–Cb). Therefore, disturbance of established apical-basolateral polarity of the gut epithelium is unlikely to be responsible for basement membrane fragmentation and IA formation in *mypt1*$^{\#4\text{-}6}$ mutants.

Actomyosin regulation is perturbed in *mypt1* mutant intestine.

Phosphorylation of MRLC regulates contractility of NMII.[15] Dephosphorylated MRLC attenuates NMII activity, limiting cytoskeletal contraction, whereas phosphorylated MRLC (pMRLC) activates NMII. Thus, contractility of NMII depends on the balance between the activity of myosin light chain kinase (MLCK) to phosphorylate MRLC and that of MLCP to dephosphorylate MRLC. Mypt1 is a regulatory subunit of MLCP that is functionally vital for MLCP's enzymatic activity. Accordingly, the level of pMRLC is expected to be higher in *mypt1* mutant embryos compared with *WT* embryos. In *WT* embryos, we observed a weak scattered distribution of pMRLC on the apical and basal side of the intestinal epithelium (Fig. 7A, C). However, as expected, the amount of pMRLC was increased in st. 25 mutant embryos compared with *WT* embryos (Fig. 7B, D), whereas the pMRLC distribution pattern could not be distinguished between mutant and *WT* embryos at st. 24 (data not shown). Of note, increased levels of pMRLC were not uniformly present along the long axis of the intestine (Fig. 7B, D). pMRLC likely accumulated in the presumptive IA lesion at st. 27 (Fig. 7D). Thus, regulation of pMRLC is significantly altered in *mypt1* mutants after at. 25, especially in the region where IA occurs.

pMRLC is bound to NMII and induces actin-myosin interaction, which results in increased contractility of the actin cytoskeleton; therefore, both increased and altered distribution of pMRLC might modify the localization of F-actin in *mypt1* mutants, probably because of altered distribution of mechanical stress.[14] In *WT* embryonic intestinal epithelial cells, F-actin was seen in the cell cortex, just beneath the plasma membrane and was slightly concentrated at the apical cell surface (Fig. 7F, H). However, whereas the intestinal canal is formed similarly in mutant and *WT* embryos, the levels of F-actin in the cell cortex appeared elevated in both the apical and basal cell surface of *mypt1* mutant embryos (Fig. 7G, I).[19] This

is consistent with increased levels of pMRLC enhancing actin fiber formation[19] and with reduced pMRLC levels resulting in decreased F-actin levels.[35,36] These data indicate that loss of *mypt1* function, followed by up-regulation of pMRLC, cause hyper-active actomyosin contraction that might be responsible for altered integrity of the intestinal epithelium, leading to IA formation in *mypt1* mutants (Fig. 7E, J).

Augmented actomyosin contraction is responsible for IA in *mypt1* mutants.

To further clarify whether augmented cytoskeletal contraction is critical for IA formation in *mypt1* mutants, we assayed whether blebbistatin, an NMII inhibitor, can rescue the IA phenotype in *mypt1*$^{\#4\text{-}6}$ mutants. When *mypt1* mutant embryos were treated with 50 μM blebbistatin at stage 25 for 2 hours, no IA phenotype was observed in any *mypt1* mutant (Fig .8A, B, Fisher's exact test, $P < 0.01$). This evidence strongly indicates that hyper-active actomyosin contraction is involved in IA development (Fig. 8C–D).

Discussion

Here we report a novel animal model of IA. Through ENU mutagenesis of medaka, we isolated the *g1-4* mutant, in which initial intestinal development proceeds appropriately but impaired integrity of the intestinal epithelium results in IA once an intestinal lumen is generated. Positional cloning identified a loss-of-function mutation in the *mypt1* gene. A mutant allele of *mypt1*$^{\#4\text{-}6}$ induced by genome editing showed a phenocopy of the *g1-4* mutant, from which we conclude that loss of *mypt1* function is responsible for the IA phenotype. In *mypt1* mutants, an increased level of pMRLC and anomalous F-actin accumulation in the developing intestine were found (Fig. 7). Inhibition of NMII significantly suppressed the IA phenotype in the *mypt1* mutant (Fig. 8), indicating that anomalously induced hyperactive cytoskeletal contraction is a plausible cause of IA. The molecular pathophysiology of human IA is largely unknown and there are few animal models of IA; therefore, the *mypt1* mutant is a valuable novel platform to better understand the molecular mechanism underlying IA.

The developmental role of Mypt1 has been documented in some species. In *Drosophila*, *mypt1* mutants have various developmental defects, including failure of dorsal closure.[37,38] In the mutant embryos, movement of the ectodermal cell sheet is disrupted and the subcellular localization of actomyosin regulatory proteins, such as pMRLC and actin, is perturbed.[37] In zebrafish *mypt1* mutants, the migration of bone morphogenetic protein 2a (*bmp2a*)-expressing lateral plate mesoderm (LPM) cells is impaired, causing agenesis/hypoplasia of the liver and exocrine pancreas.[18,22] Brain ventricle formation is also affected in the zebrafish mutant because of ectopically induced tension in the neuroepithelium layer.[19] In the mutant neuroepithelium, levels of pMRLC are aberrantly increased, resulting in unusual localization of NMII and F-actin in the neuroepithelium. Importantly, elevation and subcellular mislocalization of actomyosin regulatory components, such as pMRLC, NMII and F-actin,

are likely to be common features in *mypt1* mutants including in medaka. Furthermore, in the context of brain ventricle development in zebrafish, blebbistatin treatment to suppress MNII rescued the *mypt1* mutant phenotype. Accordingly, "epithelial relaxation" regulated by *mypt1* is probably essential for tube inflation, as occurs in brain ventricle formation. Collectively, loss of *mypt1* function affects general actomyosin dynamics during embryogenesis, and our data are consistent with this.

There are some discrepancies between the medaka *mypt1* mutants and previously reported zebrafish *mypt1* mutants. IA was not seen in zebrafish mutants, whereas neither liver nor brain ventricle aberration was observed in medaka mutants. Despite F-actin being relatively strongly accumulated in endodermal cells in zebrafish, as in medaka, the intestine of zebrafish mutants showed only mildly reduced size with normal morphology[18]. Interestingly, BMP inhibitor treatment gave rise to the phenocopy of liver-loss but did not affect the size of zebrafish intestine, indicating that reduced Bmp2a signaling caused by mislocation of *bmp2a*-expressing LPM cells is the primary reason for the liver phenotype but not for that of the intestine. The penetrance of the IA phenotype was approximately 80% (Table 2) and the size of the intestine in the medaka mutant was not reduced; therefore, a genetic modifier is likely to be involved in the discrepancy of the intestinal phenotype.

Mypt1 acts as a scaffold to provide a binding platform for assembly of the regulatory and catalytic subunits of the MLCP complex and also for the recruitment of phosphatase substrates, such as NMII. Conserved domains of Mypt1 that are vital for such molecular interaction are also found in medaka Mypt1. Our original *g1-4* mutant may provide an important clue about the function of one of these domains. The *mypt1* C2952A mutation in *g1-4* introduces a premature stop after 983 amino acids (aa), thereby deleting a large part of the PRKG interacting domain from the *WT* protein (1078 aa) (Fig 1D). The LZ motif of the PRKG interacting domain of Mypt1 specifically mediates the interaction with PRKG1α.[29] In

the regulation of vascular smooth muscle tone, activation of MLCP mediated by PRKG dephosphorylates pMRLC, which in turn induces vascular smooth muscle cell relaxation.[29] In this context, loss of the LZ motif in *g1-4* could explain increased contraction in the mutant. However, it remains to be clarified whether PRKG1α or another PRKG family member is involved in intestinal epithelium integrity.

Recently, interesting evidence regarding a human MYPT1 mutation was reported.[39] A whole exome sequencing project of 12 human holoprosencephaly spectrum and urogenital malformation patients identified *de novo* loss-of-function mutations in *MYPT1*. Among these patients, one had jejunal and ileal atresia. This case was accompanied by an aberrant mesenteric blood supply, indicating that the atresia might have been caused by accidental vascular insufficiency, which is classically hypothesized to be the pathophysiological event underlying IA. However, it cannot be completely excluded that loss of *MYPT1* function in the intestinal epithelium itself is the primary cause for IA in this human case.

Some questions remain unanswered by this study. Our data show that ectopic accumulation of pMRLC and F-actin, which likely represent a disrupted state of actomyosin cytoskeletal contraction, was not uniformly distributed over the full length of the intestine in *mypt1* mutants. We do not yet know why such an event occurs non-uniformly. In addition, we have not yet validated the molecular mechanism that underlies how hypercontractility in the intestinal epithelium disintegrates the epithelial layer structure. Further study is required to assess completely the mechanics underpinning embryonic epithelial integrity.

Experimental Procedures

Ethics statement and Fish Strains

All experiments were approved by the animal experimentation committee of Kyoto Prefectural University of Medicine (KPUM), license numbers 27-123 and 2019-154. Fish were kept at 28 °C on a 14 hours light / 10 hours dark cycle in a constant re-circulating system of the in-house KPUM facility. The d-rR medaka strain and hatching enzyme were obtained from NBRP (National Institute for Basic Biology, Okazaki, Japan). Embryos were staged according to Iwamatsu's staging system.[40]

Knock-in transgenic (KIT) medaka

To visualize the intestinal epithelium, we generated a KIT medaka line that expresses membrane-bound GFP (memGFP) under the control of the endogenous *foxa2* promotor (Fig. 3E), *Tg*[*foxa2-miniCMV:memGFP*]. *foxa2* is a well-known marker for the endoderm and its derived organs.[11] The targeting vector was constructed as described in Fig. 3.[41,42] This construct was integrated into the genome as previously described.[43] sgRNA for the genomic target site, was designed as previously described.[44] The sequences shown in Fig. 3E are as follows: CRISPR target, GTATAACCTGATACACAACAAGG; BaitD, GATCTTCGGCCTAGACTGCGAGG; minimal CMV promoter, GGTAGGCGTGTACGGTGGGAGGCCTATATAAGCAGAGCT; *Xenopus* globin 5′-UTR, CTTGTTCTTTTTGCAGAAGCTCAGAATAAACGCTCAACTTTGG; Farnesylation sequence of RAS, AAGCTGAACCCTCCTGATGAGAGTGGCCCCGGCTGCATGAGCTGCAAGTGTGTG CTCTCC; SV40 polyA signal, AACTTGTTTATTGCAGCTTATAATGGTTACAAATAAAGCAATAGCATCACAAATT

TCACAAATAAAGCATTTTTTTCACTGCATTCTAGTTGTGGTTTGTCCAAACTCATC AATGTATCTTA.

Terminal deoxynucleotidyl transferase dUTP nick end labeling (TUNEL) assay

TUNEL assays were performed using the *in situ* Apoptosis Detection Kit (Takara) according to the manufacturer's protocol. Epithelial membrane GFP signal in the intestine marked by *Tg*[*foxa2-miniCMV:memGFP*] was visualized by using rabbit anti-GFP (Invitrogen A6455) and goat anti-rabbit-IgG-Alexa633 antibodies (Thermo Fisher Scientific).

Whole mount *in situ* hybridization

A *foxa2* probe was designed and whole mount *in situ* hybridization was performed as described previously.[11 45] Template DNAs for *snai1a* (EST clone number, olea55k06), *snai1b* (olea23g07) and *snai2* (olsp48a08) were obtained from the National BioResorce Project (NBRP) medaka (https://shigen.nig.ac.jp/medaka/).

Histology

Embryos fixed with 4% paraformaldehyde were embedded in resin (Technovit 7100; Heraeus, Werheim Germany) and 6 µm tissue sections were prepared. Sections were stained with hematoxylin and analyzed using a BX51 microscope (Olympus, Tokyo, Japan).

Immunohistology

Embryos were fixed in 4% paraformaldehyde (PFA) in 1.5× PBS containing 0.1% Tween 20. Alternatively, for staining smooth muscle myosin, laminin and cytokeratin, 80% methanol/20% DMSO (Dent's solution) was used for fixation. Then, non-specific antibody binding sites were blocked with 1% dimethyl sulfoxide, 2% bovine serum albumin, 10%

normal goat serum, 0.1% Triton X-100 in 1× PBS. If Dent's fixation was used, embryos were de-chorionated with medaka hatching enzyme. Embryos fixed in PFA were permeabilized by incubation in 1× PBS containing 2% Triton X-100 for at least 2 hours before blocking of non-specific binding sites. The following commercially available antibodies were used: cytokeratin (1/100; clone AE1/AE3, ab27988; Abcam), smooth muscle myosin (1/50; BT562; Biomedical Technologies), laminin (1/100; L9393; Sigma), phospho-myosin light chain 2 (Ser19) (1:20; #3671; Cell Signaling Technology), phospho-Histone H3 (Ser10) (1/500; #06-570, Millipore), and PKCζ (1/800; ab5964; Abcam,). Alexa Fluor-633-Phalloidin (1/20; A22284; Thermo Fisher Scientific) was used to mark F-actin. Detection of primary antibodies was performed using Alexa Fluor-488, -555 goat anti-rabbit or mouse IgG (1/400; Invitrogen). To enhance the green fluorescent protein (GFP) signal, GFP-Booster Atto488 (1/100; Chromotek) was used. Images were acquired with an Olympus FV1200 confocal microscope and yz-planes were reconstructed using FIJI.[46] Abnormal accumulation of pMRLC or F-actin was judged by two criteria: (a) obviously higher immunofluorescence signal in the middle part of the intestine compared with other areas, (b) obviously higher immunofluorescence signal at apical and also basal areas of the intestinal epithelium where strong signal was never observed in the *WT*.

CRISPR/Cas9 mutagenesis of *mypt1*

The design of sgRNA for genome editing of *mypt1* exon 1 was selected using the website tool "Search for CRISPR target site with micro-homology sequences" (http://viewer.shigen.info/cgi-bin/crispr/crispr.cgi), with the parameter of "micro-homology sequences" set as "4" bases. sgRNA was prepared as previously described.[30] The sgRNA targeting sequence is shown in Fig. 2A. An RNA mixture containing 150 ng/µl sgRNA and 200 ng/µl Cas9 mRNA was injected into 1-cell embryos. Injected embryos were raised to

establish an adult F0 founder population. Genotyping of pooled F0 offspring identified eight F0 founder fish that transmitted mutations via the germ line. One of these F0 fish, #4-6 was outcrossed to *WT* fish and progeny (F1) were genotyped. The F1 fish possessing the mutation shown in Fig. S1 were used for the analysis.

Genotyping

WT and mutant *mypt1* alleles were distinguished using a polymerase chain reaction-restriction fragment length polymorphism (PCR-RFLP) method. Lysed tissue was subjected to PCR with initial denaturation at 94°C for 2 min followed by 45 cycles of 94°C denaturation for 30 s, annealing at 55°C for 30 s, and extension at 68°C for 50 s, using Quick Taq® HS DyeMix Taq polymerase (TOYOBO). The primers used were ppp1r12a-g-F15 (5′-ACCGTACATTTCCTCCACTTTCC-3′) and ppp1r2a-g-R14 (5′-TGGAATACACAGACCCGCTTTAGA-3′). PCR products were digested with *Hae*III (TOYOBO), and separated by electrophoresis in 3% agarose gels (02468-95, Nacalai) in 1× TAE buffer (Fig. 2B).

Blebbistatin treatment

To study the effects of blebbistatin on IA, st. 25 embryos were treated with 0.1% DMSO (control) or 50 μM (-)-blebbistatin (021-17041, FUJIFILM, in 0.1% DMSO). After treatment for 2 hours, embryos were washed and raised to 4 days post-fertilization (d.p.f.), and then their phenotype and genotype were elucidated.

Acknowledgements

The medaka National Bioresource Project (NBRP: https://shigen.nig.ac.jp/medaka/), governed by the Ministry of Education, Culture, Sports, Science and Technology, Japan,

provided the hatching enzyme, EST clones and the d-rR medaka strain used in this study. We thank Jeremy Allen, PhD, from Edanz (https://jp.edanz.com/ac) for editing a draft of this manuscript.

Author Contributions

DK designed the research; DK, KM, TK, SA, MK, and KN examined the mutant phenotype; DK, TK, HY, ST, TK, TK, TN and TJ performed mutant screening; YI, KA, YS and HT organized mutant screening; DK, KM, YN, MS, SS, SI, TY, HT and KY analyzed data; and DK and KY wrote the paper.

References

1. Frischer JS, Azizkhan RG. Chapter 82 - Jejunoileal Atresia and Stenosis. In: Coran AG, ed. *Pediatric Surgery (Seventh Edition)*. Philadelphia: Mosby; 2012:1059-1071.

2. Louw JH, Barnard CN. Congenital intestinal atresia; observations on its origin. *Lancet*. Nov 19 1955;269(6899):1065-7. https://doi.org10.1016/s0140-6736(55)92852-x.

3. Louw JH. Congenital intestinal atresia and stenosis in the newborn. Observations on its pathogenesis and treatment. *Ann R Coll Surg Engl*. Nov 1959;25:209-34.

4. Shorter NA, Georges A, Perenyi A, Garrow E. A proposed classification system for familial intestinal atresia and its relevance to the understanding of the etiology of jejunoileal atresia. *Journal of pediatric surgery*. 2006/11/01/ 2006;41(11):1822-1825. https://doi.orghttps://doi.org/10.1016/j.jpedsurg.2006.06.008.

5. Celli J. Genetics of gastrointestinal atresias. *European journal of medical genetics*. Aug 2014;57(8):424-439. https://doi.org10.1016/j.ejmg.2014.06.007.

6. Gupta T, Yang W, Iovannisci DM, et al. Considering the vascular hypothesis for the pathogenesis of small intestinal atresia: a case control study of genetic factors. *Am J Med Genet A*. Apr 2013;161A(4):702-10. https://doi.org10.1002/ajmg.a.35775.

7. Fairbanks TJ, Kanard R, Del Moral PM, et al. Fibroblast growth factor receptor 2 IIIb invalidation--a potential cause of familial duodenal atresia. *Journal of pediatric surgery*. Jun 2004;39(6):872-4. https://doi.org10.1016/j.jpedsurg.2004.02.026.

8. Fairbanks TJ, Kanard RC, De Langhe SP, et al. A genetic mechanism for cecal atresia: the role of the Fgf10 signaling pathway. *J Surg Res*. Aug 2004;120(2):201-9. https://doi.org10.1016/j.jss.2003.12.017.

9. Fairbanks TJ, Kanard RC, Del Moral PM, et al. Colonic atresia without mesenteric vascular occlusion. The role of the fibroblast growth factor 10 signaling pathway. *Journal of pediatric surgery*. Feb 2005;40(2):390-6. https://doi.org10.1016/j.jpedsurg.2004.10.023.

10. Kanard RC, Fairbanks TJ, De Langhe SP, et al. Fibroblast growth factor-10 serves a regulatory role in duodenal development. *Journal of pediatric surgery*. Feb 2005;40(2):313-6. https://doi.org10.1016/j.jpedsurg.2004.10.057.

11. Kobayashi D, Jindo T, Naruse K, Takeda H. Development of the endoderm and gut in medaka, Oryzias latipes. *Dev Growth Differ*. Jun 2006;48(5):283-95.

12. Munjal A, Lecuit T. Actomyosin networks and tissue morphogenesis. *Development*. May 2014;141(9):1789-93. https://doi.org10.1242/dev.091645.

13. Agarwal P, Zaidel-Bar R. Principles of Actomyosin Regulation In Vivo. *Trends Cell Biol*. Oct 29 2018. https://doi.org10.1016/j.tcb.2018.09.006.

14. Vicente-Manzanares M, Ma X, Adelstein RS, Horwitz AR. Non-muscle myosin II takes centre stage in cell adhesion and migration. *Nature reviews*. Nov 2009;10(11):778-90. https://doi.org10.1038/nrm2786.

15. Ito M, Nakano T, Erdodi F, Hartshorne DJ. Myosin phosphatase: structure, regulation and function. *Mol Cell Biochem*. Apr 2004;259(1-2):197-209. https://doi.org10.1023/b:mcbi.0000021373.14288.00.

16. Grassie ME, Moffat LD, Walsh MP, MacDonald JA. The myosin phosphatase targeting protein (MYPT) family: a regulated mechanism for achieving substrate specificity of the catalytic subunit of protein phosphatase type 1delta. *Arch Biochem Biophys*. Jun 15 2011;510(2):147-59. https://doi.org10.1016/j.abb.2011.01.018.

17. Hartshorne DJ, Ito M, Erdodi F. Role of protein phosphatase type 1 in contractile functions: myosin phosphatase. *J Biol Chem*. Sep 3 2004;279(36):37211-4. https://doi.org10.1074/jbc.R400018200.

18. Huang H, Ruan H, Aw MY, et al. Mypt1-mediated spatial positioning of Bmp2-producing cells is essential for liver organogenesis. *Development*. Oct 2008;135(19):3209-18. https://doi.org10.1242/dev.024406.

19. Gutzman JH, Sive H. Epithelial relaxation mediated by the myosin phosphatase regulator Mypt1 is required for brain ventricle lumen expansion and hindbrain morphogenesis. *Development*. Mar 2010;137(5):795-804. https://doi.org10.1242/dev.042705.

20. Weiser DC, Row RH, Kimelman D. Rho-regulated myosin phosphatase establishes the level of protrusive activity required for cell movements during zebrafish gastrulation. *Development*. Jul 2009;136(14):2375-84. https://doi.org10.1242/dev.034892.

21. Kim JH, Lee SR, Li LH, et al. High cleavage efficiency of a 2A peptide derived from porcine teschovirus-1 in human cell lines, zebrafish and mice. *PLoS One*. 2011;6(4):e18556. https://doi.org10.1371/journal.pone.0018556.

22. Dong G, Huang Y, Ding H, et al. Mypt1 regulates Bmp signaling to promote embryonic exocrine pancreas growth in zebrafish. *Genesis*. Nov 8 2019:e23345. https://doi.org10.1002/dvg.23345.

23. Barresi MJ, Burton S, Dipietrantonio K, Amsterdam A, Hopkins N, Karlstrom RO. Essential genes for astroglial development and axon pathfinding during zebrafish embryogenesis. *Dev Dyn*. Oct 2010;239(10):2603-18. https://doi.org10.1002/dvdy.22393.

24. Angulo-Urarte A, Casado P, Castillo SD, et al. Endothelial cell rearrangements during vascular patterning require PI3-kinase-mediated inhibition of actomyosin contractility. *Nat Commun*. Nov 16 2018;9(1):4826. https://doi.org10.1038/s41467-018-07172-3.

25. Okamoto R, Ito M, Suzuki N, et al. The targeted disruption of the MYPT1 gene results in embryonic lethality. *Transgenic research*. Jun 2005;14(3):337-40. https://doi.org10.1007/s11248-005-3453-3.

26. Yokoi H, Shimada A, Carl M, et al. Mutant analyses reveal different functions of fgfr1 in medaka and zebrafish despite conserved ligand-receptor relationships. *Dev Biol*. Apr 1 2007;304(1):326-37. https://doi.org10.1016/j.ydbio.2006.12.043.

27. Aghaallaei N, Gruhl F, Schaefer CQ, et al. Identification, visualization and clonal analysis of intestinal stem cells in fish. *Development*. Oct 1 2016;143(19):3470-3480. https://doi.org10.1242/dev.134098.

28. Kimura T, Jindo T, Narita T, et al. Large-scale isolation of ESTs from medaka embryos and its application to medaka developmental genetics. *Mech Dev*. Jul 2004;121(7-8):915-32. https://doi.org10.1016/j.mod.2004.03.033.

29. Surks HK, Mochizuki N, Kasai Y, et al. Regulation of myosin phosphatase by a specific interaction with cGMP- dependent protein kinase Ialpha. *Science*. Nov 19 1999;286(5444):1583-7. https://doi.org10.1126/science.286.5444.1583.

30. Ansai S, Kinoshita M. Targeted mutagenesis using CRISPR/Cas system in medaka. *Biology open*. Apr 11 2014. https://doi.org10.1242/bio.20148177.

31. Wallace KN, Akhter S, Smith EM, Lorent K, Pack M. Intestinal growth and differentiation in zebrafish. *Mech Dev*. Feb 2005;122(2):157-73. https://doi.org10.1016/j.mod.2004.10.009.

32. Yang J, Antin P, Berx G, et al. Guidelines and definitions for research on epithelial-mesenchymal transition. *Nature reviews*. Jun 2020;21(6):341-352. https://doi.org10.1038/s41580-020-0237-9.

33. Savagner P. Epithelial-mesenchymal transitions: from cell plasticity to concept elasticity. *Current topics in developmental biology*. 2015;112:273-300. https://doi.org10.1016/bs.ctdb.2014.11.021.

34. Scheibner K, Schirge S, Burtscher I, et al. Epithelial cell plasticity drives endoderm formation during gastrulation. *Nature Cell Biology*. 2021/07/01 2021;23(7):692-703. https://doi.org10.1038/s41556-021-00694-x.

35. Ray RM, Guo H, Patel M, Jin S, Bhattacharya S, Johnson LR. Role of myosin regulatory light chain and Rac1 in the migration of polyamine-depleted intestinal epithelial cells. *Am J Physiol Gastrointest Liver Physiol*. Apr 2007;292(4):G983-95. https://doi.org10.1152/ajpgi.00356.2006.

36. Bavaria MN, Ray RM, Johnson LR. The phosphorylation state of MRLC is polyamine dependent in intestinal epithelial cells. *Am J Physiol Cell Physiol*. Jan 2011;300(1):C164-75. https://doi.org10.1152/ajpcell.00247.2010.

37. Mizuno T, Tsutsui K, Nishida Y. Drosophila myosin phosphatase and its role in dorsal closure. *Development*. Mar 2002;129(5):1215-23. https://doi.orghttps://doi.org/10.1242/dev.129.5.1215.

38. Tan C, Stronach B, Perrimon N. Roles of myosin phosphatase during Drosophila development. *Development*. Feb 2003;130(4):671-81. https://doi.org10.1242/dev.00298.

39. Hughes JJ, Alkhunaizi E, Kruszka P, et al. Loss-of-Function Variants in PPP1R12A: From Isolated Sex Reversal to Holoprosencephaly Spectrum and Urogenital Malformations. *American journal of human genetics*. Jan 2 2020;106(1):121-128. https://doi.org10.1016/j.ajhg.2019.12.004.

40. Iwamatsu T. Stages of normal development in the medaka Oryzias latipes. *Mech Dev*. Jul 2004;121(7-8):605-18. https://doi.org10.1016/j.mod.2004.03.012.

41. Okuyama T, Isoe Y, Hoki M, et al. Controlled Cre/loxP site-specific recombination in the developing brain in medaka fish, Oryzias latipes. *PLoS One*. 2013;8(6):e66597. https://doi.org10.1371/journal.pone.0066597.

42. Ansai S, Kinoshita M. Genome Editing of Medaka. *Methods in molecular biology*. 2017;1630:175-188. https://doi.org10.1007/978-1-4939-7128-2_15.

43. Murakami Y, Ansai S, Yonemura A, Kinoshita M. An efficient system for homology-dependent targeted gene integration in medaka (Oryzias latipes). *Zoological letters*. 2017;3:10. https://doi.org10.1186/s40851-017-0071-x.

44. Kimura Y, Hisano Y, Kawahara A, Higashijima S. Efficient generation of knock-in transgenic zebrafish carrying reporter/driver genes by CRISPR/Cas9-mediated genome engineering. *Scientific reports*. 2014;4:6545. https://doi.org10.1038/srep06545.

45. Takashima S, Shimada A, Kobayashi D, et al. Phenotypic analysis of a novel chordin mutant in medaka. *Dev Dyn*. Aug 2007;236(8):2298-310. https://doi.org10.1002/dvdy.21245.

46. Schindelin J, Arganda-Carreras I, Frise E, et al. Fiji: an open-source platform for biological-image analysis. *Nature methods*. Jun 28 2012;9(7):676-82. https://doi.org10.1038/nmeth.2019.

47. Parkin CA, Allen CE, Ingham PW. Hedgehog signalling is required for cloacal development in the zebrafish embryo. *The International journal of developmental biology*. 2009;53(1):45-57. https://doi.org10.1387/ijdb.082669cp.

Figure Legends

Fig. 1. Characterization of medaka IA mutant, *g1-4*.

(A, B) Lateral views of *WT* (A) and *mypt1* mutant (*g1-4*) (B) embryos at st. 40. Note IA developed in the mutant, represented by the blind ends of the intestine (arrowheads). Anterior is to the left. Arrow, cloaca; GB, gallbladder; Dotted brackets, intestine. Scale bar: 200 µm. (C) Schematic presentation of part of LG23. The *g1-4* locus is confined to a 0.13 cM interval between the markers LG23-4.4 and LG23-4.6. Inset: chromatogram of a point mutation in *g1-4*, which gives rise to a premature stop codon. (D) Schematics outlining Mypt1 domains of *WT* (top), *g1-4* (middle), and *mypt1*$^{\#4\text{-}6}$ (bottom) proteins. Translation termination positions are indicated by *. In *mypt1*$^{\#4\text{-}6}$, an 11 nucleotide deletion with a 7 nucleotide insertion causes a frame-shift (green) and a truncated coding sequence.

Fig. 2. Comparison of *WT* and *mypt1*$^{\#4\text{-}6}$ allele sequences.

(A) The 11 nucleotide deletion and 7 nucleotide insertion are shown in red and blue, respectively. The CRISPR target site is underlined. The predicted amino acid sequence resulting from the frame shift is shown in green. Asterisk indicates premature translation termination. *Hae*III recognition sites (GGCC) that are used for genotyping by restriction fragment length polymorphism assays are indicated. (B) Schematic outline of PCR products amplified from *WT* and *mypt1*$^{\#4\text{-}6}$ alleles. Primer positions (ppp1r12a-F15 and ppp1r12a-

R16), the CRISPR target site and *Hae*III recognition sites are indicated. The *Hae*III site lost in *mypt1*$^{\#4\text{-}6}$ is shown in gray. The position of the introduced stop codon in *mypt1*$^{\#4\text{-}6}$ is shown by an asterisk.

Fig. 3 The embryonic intestine in *WT* and *mypt1*$^{\#4\text{-}6}$ animals

(A–D) Dilation of the intestine in *mypt1* mutants. Ventral view of *WT* (A and B) or *mypt1*$^{\#4\text{-}6}$ (C and D) st. 40 embryos in the *Tg*[*foxa2-miniCMV:memGFP*] medaka line. GFP signal and bright field views are shown in (A, B) and (C, D), respectively. The outlines of the intestine are traced by white dotted lines. Note the intestine anterior to the IA lesion was significantly dilated in the *mypt1* mutant (asterisk). LV, liver. Scale bar: 200 µm. (E) CRISPR/Cas9-mediated KIT generation strategy. (F–M) Histological micrographs of the *WT* (F–I) and *mypt1*$^{\#4\text{-}6}$ (J–M) intestine of st. 32 embryos stained with hematoxylin. (J) Region anterior to the atresia, (K) atresia lesion, (L) anterior blind-end of the remaining part of the posterior intestine and (M) region posterior to the atresia region. (F–I) correspond to (J–M) as almost the same positions, respectively. Note the morphology looks intact in (I) and (L). MS, mesentery; NT, nephric tubule. Scale bar: 20 µm.

Fig. 4. Apical-basolateral polarity is not perturbed in *mypt1* mutants

(A) Schematic diagram of the distribution of cytokeratin, laminin and smooth muscle (SM) myosin in the developing intestine. (B–G) Whole mount immunofluorescence micrographs of cytokeratin and SM myosin (B and C), and laminin (D–G) of *WT* (B, D, and F) and *mypt1*$^{\#4\text{-}6}$ animals with C, E, and G as lateral views (Left; anterior). White dotted lines indicate the outline of the embryonic intestine in a differential interference contrast (DIC) micrograph corresponding to a fluorescence image. Note that basement membrane was fragmented in the mutant embryos at st. 26 before IA had obviously appeared (Gb). (H, I)

Immunohistochemistry for Pkcζ in long-axis optical sections of st. 26 embryo intestines. The epithelium of the intestine was visualized with *Tg*[*foxa2-miniCMV:memGFP*] (Ha and Ia). Note that the apical localization of Pkcζ was not disturbed in *mypt1* mutants (Ib). Data are representative of six and four embryos for *WT* and mutants, respectively. Left side; anterior. Arrowheads, blind-ends of IA. Scale bars: (B–E, H, I) 50 µm, (F, G) 20 µm.

Fig. 5. Endodermal migration to form the intestinal anlage is intact in *mypt1* mutants.
WT (A, C, E, G, I, K) and *mypt1* mutant (B, D, F, H, J, L) embryos were subjected to whole mount *in situ* hybridization for *foxa2*. Dorsal (A–D) and dorsolateral views (E–H) are shown. Embryonic stages are indicated in the lower left. The outlines of the forming intestine are traced by white dotted lines. Note, until st. 26, the intestinal anlage represented by *fox2a* seems normal in the mutants (B, D, F, H and J). At st. 27, the anlage shows a gap in continuity of the intestinal anlage along the anteroposterior axis (arrowheads). Scale bar: 100 µm.

Fig. 6. Cell death, cell proliferation and epithelial-mesenchymal transition are not involved in IA development.
(A–D) Cell death and cell proliferation in the intestine are not significantly affected in *mypt1* mutants. (A, B) TUNEL assays of *WT* (A) and *mypt1* mutant (B) embryos at st. 26. Dotted ellipses indicate a number of apoptotic cells surrounding the cloaca opening where apoptosis is always observed.[47] (C–H) *WT* (C, E, G) and *mypt1* mutant (D, F, H) embryos at stage 25 were stained with anti-phosphorylated histone H3 (PH3) antibody and/or propidium iodide (PI). (I) The ratio of PH3-positive cells to total cell number (*WT*, n=11; mutant, n=3, χ-square test, $P > 0.05$). Scale bar: 50 µm. (J–O) EMT is not involved in IA formation in *mypt1* mutants. Lateral views of st. 26 embryos processed for whole mount *in situ* hybridization to

detect EMT markers. *WT* and *mypt1* mutants are shown in (J, L, N) and (K, M, O), respectively; (J, K) for *snai1a*, (L, M) for *snai1b*, and (N, O) for *snai2*. Intestines are outlined by dotted lines. Scale bar: 50 µm. Note no signal of *snai1a*, *snai1b* and *snai2*.

Fig. 7. Actomyosin is activated in the developing intestine of *mypt1* mutants

(A–D) Fluorescence micrographs of pMRLC for *WT* (A and C) and *mypt1*$^{\#4\text{-}6}$ (B and D). st. 25 embryos are shown in A and B, whereas st. 27 embryos are shown in C and D. Scale bar, 25 µm. Note significant accumulation of pMRLC in mutant intestinal epithelium (B and D). (E) The proportion of embryos possessing an abnormal increase of pMRLC in embryonic intestine (Fisher's exact test, $P < 0.01$). (F–I) Fluorescence micrographs of F-actin stained with phalloidin. (a–e) represent short axis sections of intestine. *WT* (F, H) and *mypt1*$^{\#4\text{-}6}$ (G, I) st.25 (F, G) and st. 27 (H, I) embryos are shown. (J) Abnormal accumulation of F-actin in the *mypt1* mutant intestine. Consistent with pMRLC data, F-actin was accumulated in the mutant epithelium. Scale bar: 25 µm. *, an intestinal lumen (Fisher's exact test, $P < 0.01$).

Fig. 8. Attenuation of actomyosin activation rescues the IA phenotype in *mypt1* mutants.

(A) Experimental outline of blebbistatin treatment. (B) Quantification of the rescue of the IA phenotype in *mypt1*$^{\#4\text{-}6}$ embryos by treatment with blebbistatin (Fisher's exact test, $P < 0.01$). (C) Schematic representation of the core module to regulate NMII activity. Note, Mypt1 is a key component of MLCP and is essential for MLCP activity. Loss of Mypt1 function reduces MLCP activity, followed by the ectopic activation of actomyosin contraction. (D) Hypothetical molecular event following loss of *mypt1* function. (F) Schematic representation under blebbistatin treatment.

Table 1. Variation in penetrance among *g1-4* pairs

Fish pair		IA	TOTAL	%
Female 1	Male 1	1	37	2.7
Female 2	Male 2	8	45	17.8
Female 2	Male 3	8	36	22.2
Female 3	Male 2	5	30	16.7
Female 4	Male 3	2	20	10.0
Female 5	Male 1	4	45	8.9

IA: The number of embryos that develop intestinal atresia.

Total: The number of embryos after deduction of those for which intestinal phenotype could not be determined (dead or abnormal development) .

Table 2. Variation in penetrance among *mypt1* $^{\#4\text{-}6}$ pairs

Generation	Fish pair		IA	TOTAL	%
	Female	Male			
F1	16	17	14	59	23.7
F2	33	34	19	97	19.6
	35	36	9	29	31.0
	37	38	8	30	26.7
	39	40	13	71	18.3
	41	43	13	84	15.5
	44	45	9	44	20.5
	46	47	17	62	27.4
	48	49	13	90	14.4
	50	51	12	72	16.7
	54	55	5	39	12.8
	56	57	15	83	18.1
F2 average			133	701	19.0

IA: The number of embryos that develop intestinal atresia.

Total: The number of embryos after deduction of those for which intestinal phenotype could not be determined (dead or abnormal development) .

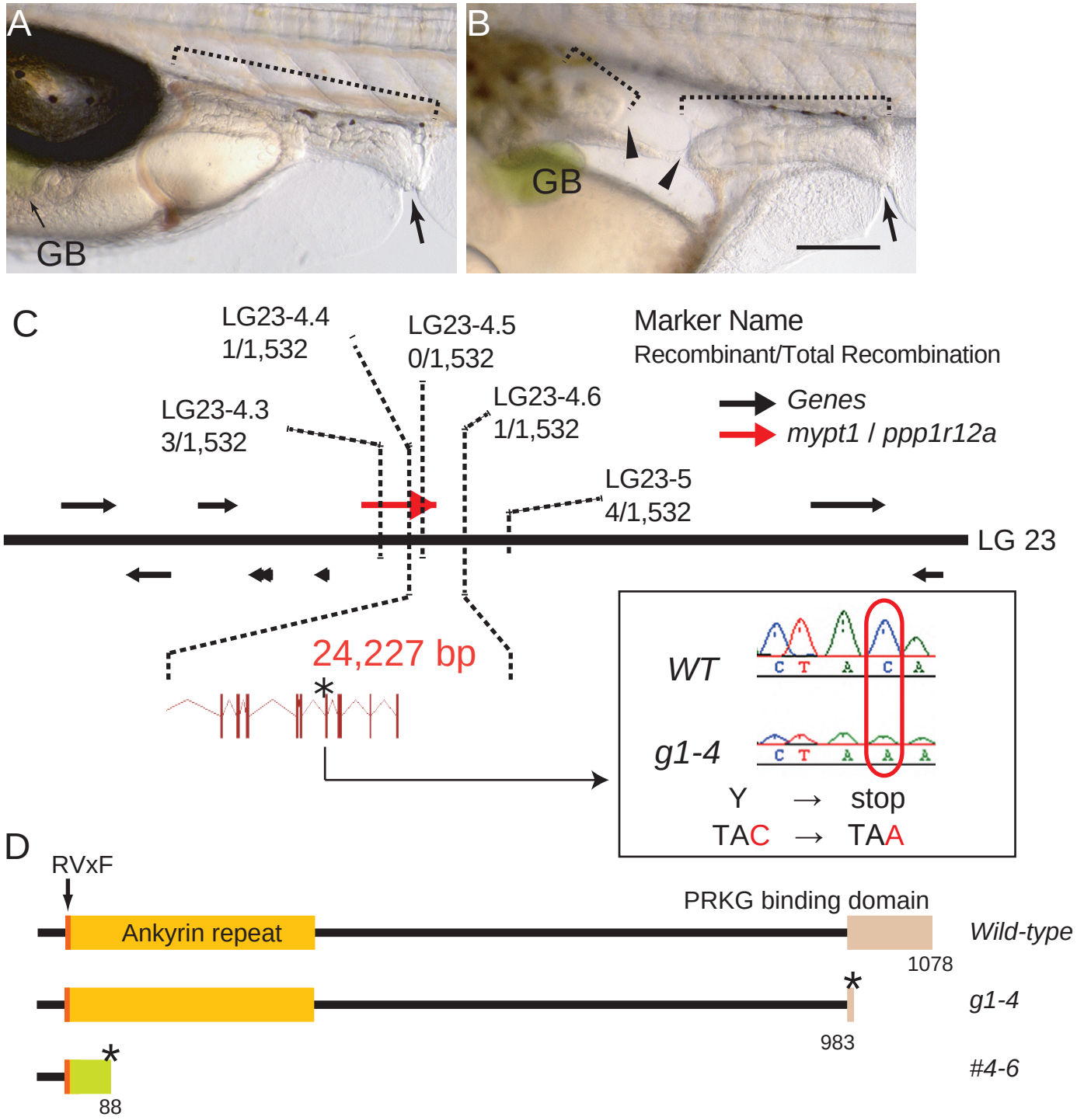

Fig. 1. characterization of medaka IA mutant *g1-4*

A

```
                    10        20        30        40        50        60
WT          ATGAAGATGGCGGACGCCAAGCAGAAAAGGAATGAACAGCTAAAGCGATGGATGGGCTCG
            M  K  M  A  D  A  K  Q  K  R  N  E  Q  L  K  R  W  M  G  S

                    70        80        90       100       110       120
mypt1#4-6   GAAACGGACCAGGAGCCTCCTGTTTTCAAAAAGAAGAAGACGAAGGTGAAGTTCGATGAT
              E  T  D  Q  E  P  P  V  F  K  K  K  K  T  K  V  K  F  D  D
                          HaeIII
                   130       140       150       160       170       180
WT          GGCGCCGTGTTTCTGGCCGCCTGCTCAAGCGGCGATACAGAGGAGGTGCTCCGTATGCTG
              G  A  V  F  L  A  A  C  S  S  G  D  T  E  E  V  L  R  M  L
mypt1#4-6   GGCGCCTCTGTAT----CGCCTGCTCAAGCGGCGATACAGAGGAGGTGCTCCGTATGCTG
              G  A  S  V  S      P  A  Q  A  A  I  Q  R  R  C  S  V  C  W
                 in/del                          HaeIII
                   190       200       210       220       230       240
WT          GACCGGGGTGCTGACATCAACTATGCCAATGTGGACGGCCTCACAGCGCTCCACCAGGCA
              D  R  G  A  D  I  N  Y  A  N  V  D  G  L  T  A  L  H  Q  A
mypt1#4-6   GACCGGGGTGCTGACATCAACTATGCCAATGTGGACGGCCTCACAGCGCTCCACCAGGCA
               T  G  V  L  T  S  T  M  P  M  W  T  A  S  Q  R  S  T  R  H

                             250       260
WT          TGCATCGACGACAACGTGGACATGGTGA
            C  I  D  D  N  V  D  M  V
mypt1#4-6   TGCATCGACGACAACGTGGACATGGTGA
             A  S  T  T  T  W  T  W  *
```

B

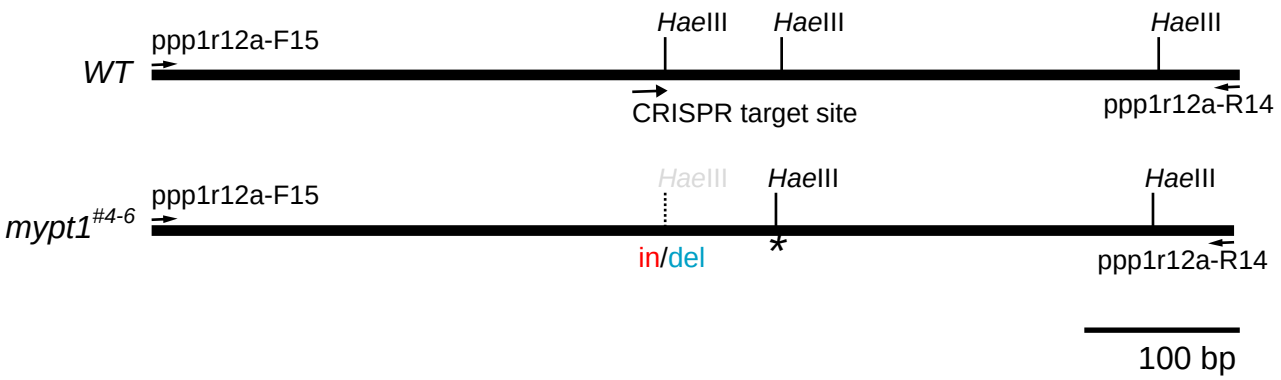

Fig. 2. Comparison of WT and *mypt1*$^{\#4\text{-}6}$ mutant allele sequence.

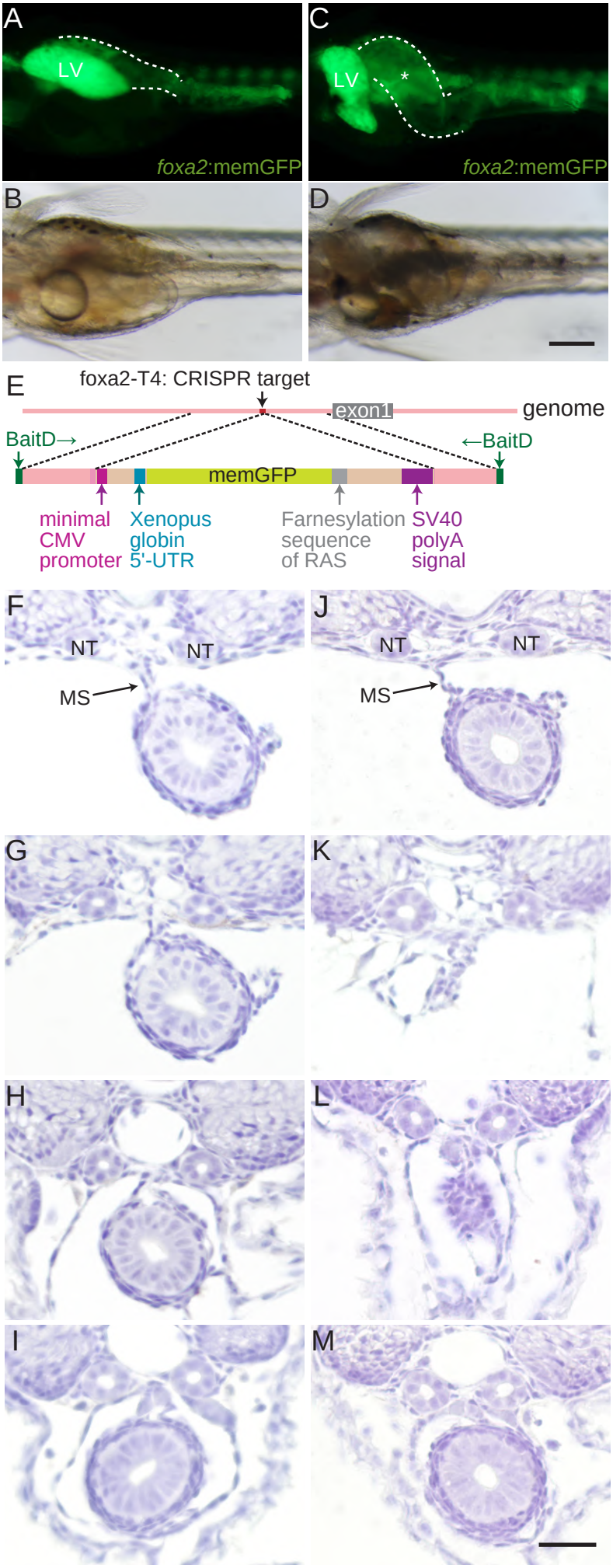

Fig. 3 The embryonic intestine in the *WT* and *mypt1*$^{\#4\text{-}6}$.

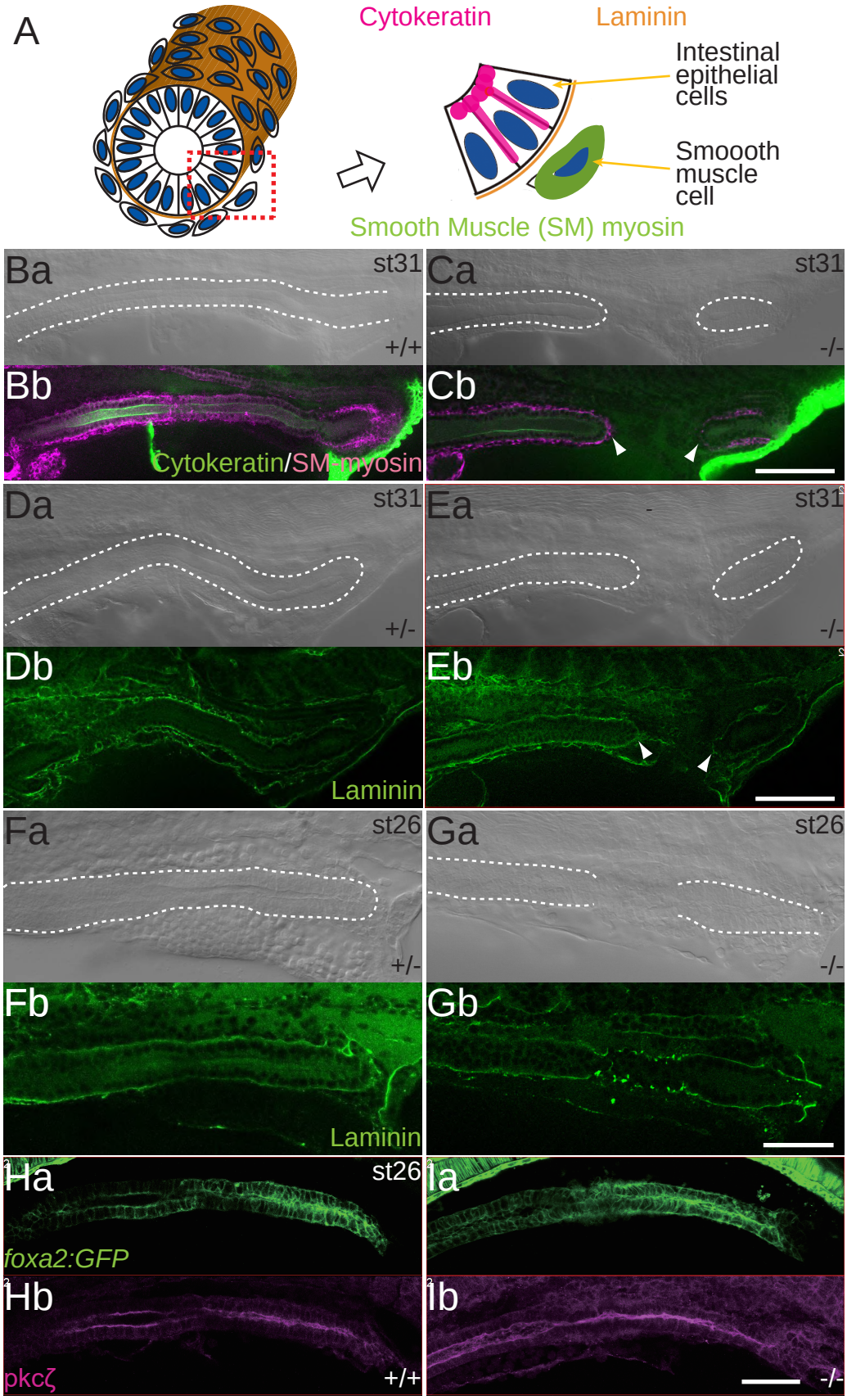

Fig. 4. Apical-basolateral polarity is not perturbed in *mypt1* mutant

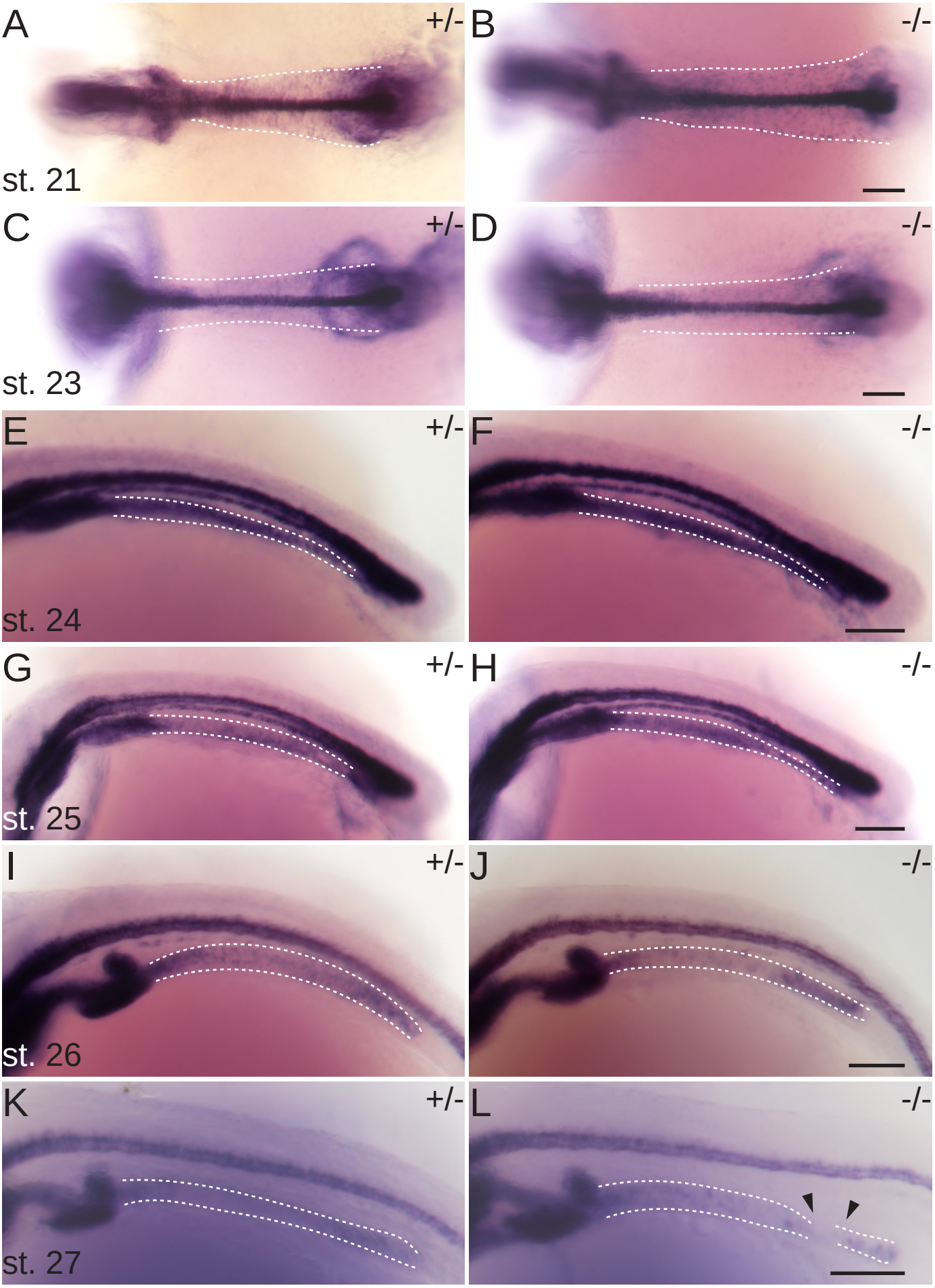

Fig. 5 Endodermal migration to form intestinal anlage is intact in *mypt1* mutant.

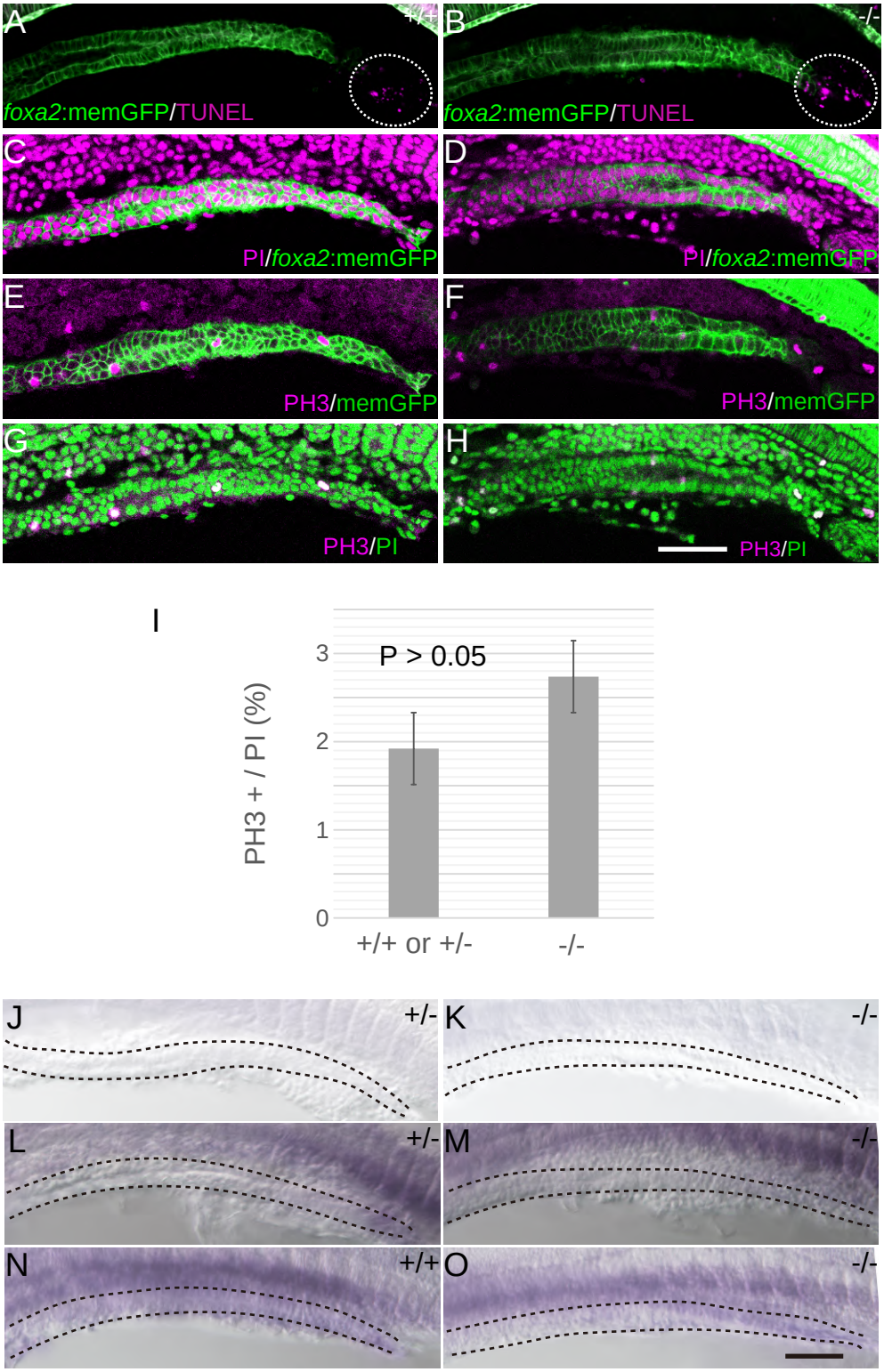

Fig. 6. Cell death, cell proliferation and epithelial-mesenchymal transition are not involved in IA development.

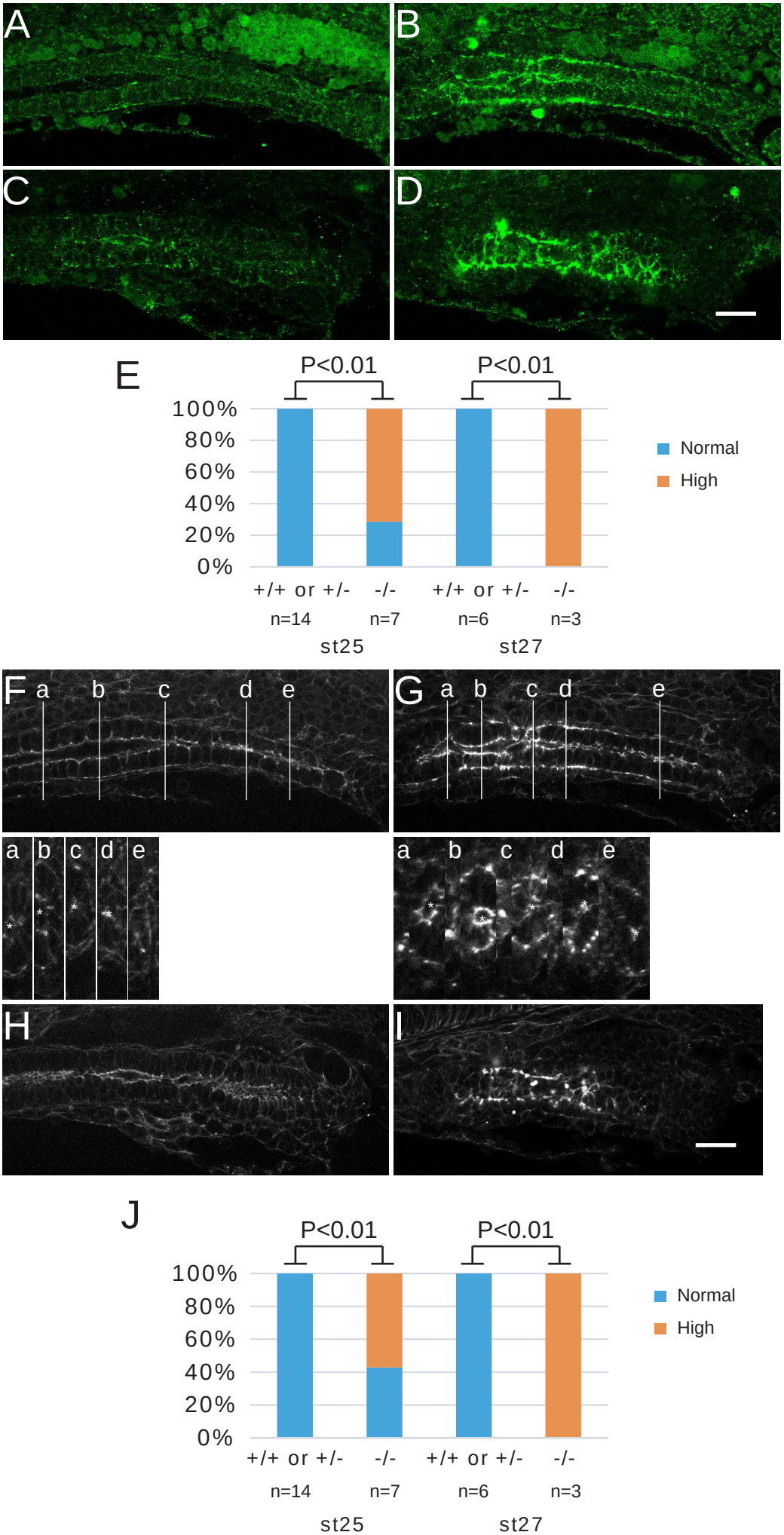

Fig. 7. Actomyosin is activated in the developing intestine of *mypt1* mutant

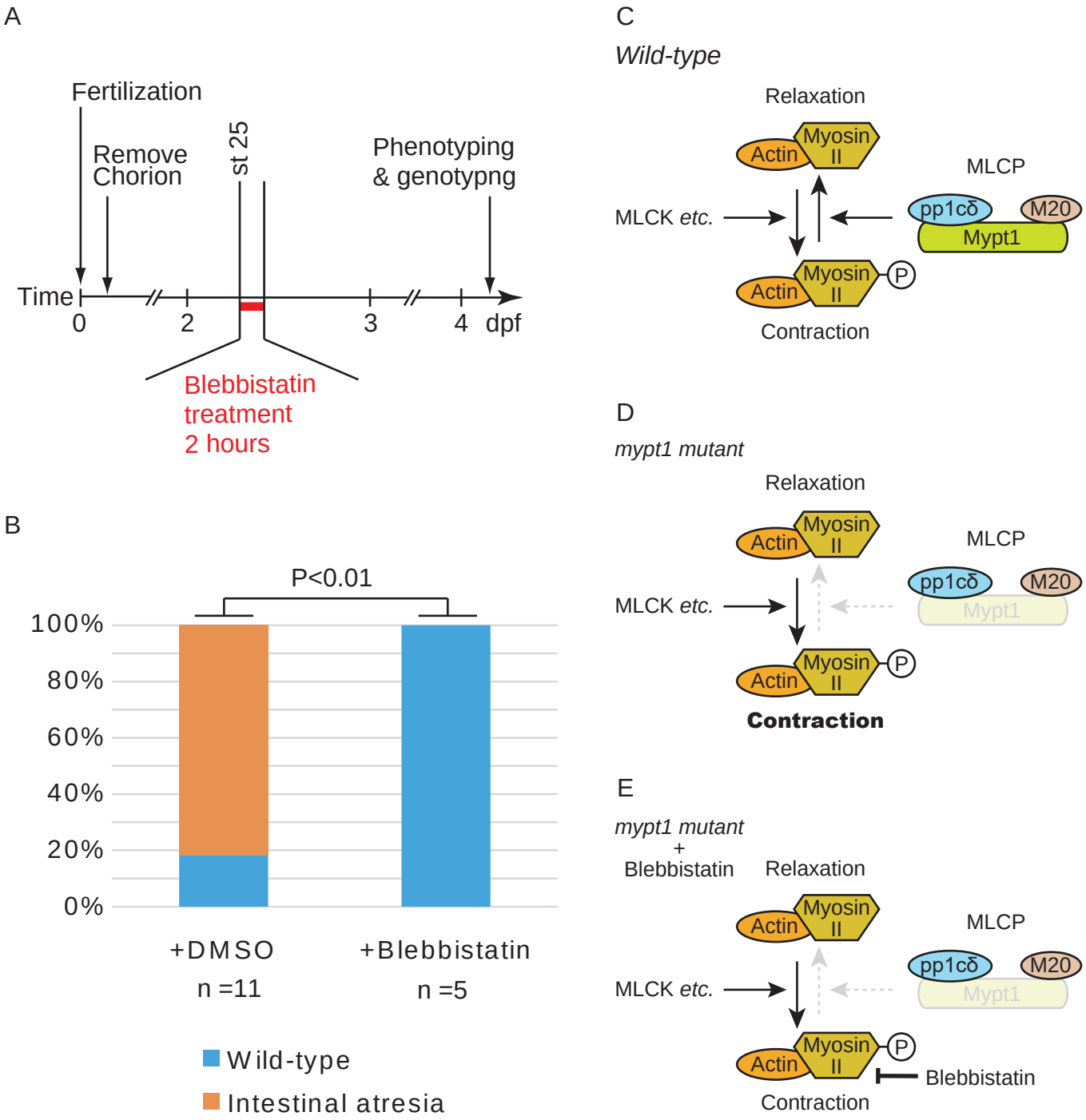

Fig. 8. Attenuation of actomyosin activation rescues IA phenotype in *mypt1* mutants.